Magnetic field effect on nuclear matter from a Skyrmion crystal model

Mamiya Kawaguchi,[1,*] Yong-Liang Ma,[2,†] and Shinya Matsuzaki[1,2,‡]
[1]*Department of Physics, Nagoya University, Nagoya 464-8602, Japan*
[2]*Center for Theoretical Physics and College of Physics, Jilin University, Changchun 130012, China*

(Received 25 May 2018; published 26 September 2018)

We explore magnetic field effects on the nuclear matter based on the Skyrmion crystal approach for the first time. It is found that the magnetic effect plays the role of a catalyzer for the topology transition in the baryonic matter. Furthermore, we observe that in the presence of the magnetic field, the inhomogeneous chiral condensate persists in both the Skyrmion and the half-Skyrmion phases. Explicitly, as the strength of magnetic field gets larger, the inhomogeneous chiral condensate in the Skyrmion phase tends to be drastically localized, while in the half-Skyrmion phase the inhomogeneity configuration is hardly affected. It also turns out that a large magnetic effect in a low-density region distorts the baryon shape to an elliptic form but the crystal structure is intact. However, in a high-density region, the crystal structure is strongly affected by the strong magnetic field. A possible correlation between the chiral inhomogeneity and the deformation of the Skyrmion configuration is also addressed. The results obtained in this article might be realized in the deep interior of compact stars.

DOI: 10.1103/PhysRevC.98.035803

I. INTRODUCTION

Exploring the phase diagram of QCD under an external magnetic source is an active and a significant field in high-energy physics relevant to the heavy-ion physics, compact stars, and the evolution of the early universe (see, e.g., Ref. [1] for a recent review and references therein). Studies of this kind have been performed using various effective theories and models based on chiral perturbation theory [2–5] and the Nambu-Jona-Lasinio model [6–10]. In the present work, we make the first attempt to study the magnetic effect on the nuclear matter based on the Skyrmion crystal model.

In the Skyrmion crystal approach baryons arise as the topological objects in a nonlinear mesonic theory—the Skyrmions-Skyrme model [11], and the nuclear matter is simulated by putting the Skyrmions onto the crystal lattice and regarding the nuclear matter as the Skyrmion matter [12]. [In the present analysis, we specifically choose the face-centered-cubic (fcc) crystal.] In this approach, the nuclear matter, medium-modified hadron properties and the symmetry-breaking patterns in a dense system can be accessed in a unified way [13–16] (for a recent review, see, e.g., Ref. [17]).

In this article, we include the magnetic field in the Skyrmion crystal approach for the first time to study the magnetic effect on the nuclear matter with interest particularly in the topology transition in the baryonic matter (to be specified later), the inhomogeneous quark condensate, and the shape of a single baryon (Skyrmion). What we have done and found can be summarized as follows.

(i) The magnetic effect plays the role of a catalyzer for the topology transition in the baryonic matter (deformation of the crystal configuration from a face-centered-cubic Skyrmion crystal to a cubic-centered half-Skyrmion crystal[1]). The baryon energy per Skyrmion (soliton mass) is enhanced by the presence of the magnetic field.

(ii) Regarding the magnetic field dependence of the inhomogeneity of the chiral condensate in a medium modeled by the Skyrmion crystal, it turns out that, even in the presence of the magnetic field, the inhomogeneous chiral condensate persists in both the Skyrmion and the half-Skyrmion phases. Interestingly enough, as the strength of the magnetic field gets larger, the inhomogeneous chiral condensate in the Skyrmion phase tends to be drastically localized, while in the half-Skyrmion phase the inhomogeneity configuration is almost intact. (Similar observations, regarding the deformation of inhomogeneities for the chiral condensate by magnetic effects, have been made in different models [18–21].)

(iii) As to the magnetic effect on the Skyrmion configuration and the single baryon's shape in the medium, it is found that a large magnetic strength in a low-density

*mkawaguchi@hken.phys.nagoya-u.ac.jp
†yongliangma@jlu.edu.cn
‡synya@hken.phys.nagoya-u.ac.jp

[1]Actually, this topology transition is not like an ordinary phase transition, because it is not characterized by a continuous symmetry structure, i.e., an order parameter for spontaneous symmetry breaking. Nevertheless, we conventionally call it a phase transition throughout this article.

region (in the Skyrmion phase) makes the baryon's shape be elliptic, while the crystal configuration essentially holds. In contrast, in a high-density region (in the half-Skyrmion phase), the crystal structure is significantly affected by the existence of a large magnetic field.

(iv) A correlation between the chiral inhomogeneity and the deformation of the Skyrmion crystal configuration can be seen through a nontrivial deformation due to a large magnetic field, which would be a novel indirect probe for the presence of the inhomogeneity of the chiral condensate in the half-Skyrmion phase.

We anticipate that our findings as listed above might affect the equation of state of dense nuclear matter or compact stars having a strong magnetic field. Such characteristic features possibly emergent in dense matter or compact stars could be (indirectly) tested by future astronomical observations.

This article is organized as follows. In Sec. II we introduce the basic setup for studying magnetic properties of the Skyrmion crystal. With this preliminary setup at hand, in Sec. III we show our numerical analysis for the magnetic dependencies on the Skyrmion crystal and some related phenomena such as the topology transition in the baryonic matter, the inhomogeneous chiral condensates, and the deformation of a single baryon's shape. Section IV is devoted to a summary of our study and findings. The Appendix provides detailed computations regarding some prescriptions for the crystal configuration under the magnetic effect.

II. THE MODEL OF SKYRMION CRYSTAL IN A MAGNETIC FIELD

In this section, we first give a brief summary of the basics of the Skyrmion crystal model related to the present work following Ref. [13], and then we introduce the basic strategy for studying the magnetic properties of the Skyrmion crystal.

A. Skyrmion crystal

We begin by considering the following Skyrme model Lagrangian [11]:

$$\mathcal{L}_{\rm Skyr} = \frac{f_\pi^2}{4}{\rm tr}[\partial_\mu U \partial^\mu U^\dagger] + \frac{1}{32g^2}{\rm tr}[U^\dagger\partial_\mu U, U^\dagger \partial_\nu U]^2, \quad (1)$$

where U is the chiral field embedding the pion fields, f_π is the pion-decay constant, and g is the dimensionless coupling constant, the Skyrme parameter. In the Skyrmion crystal approach, it is convenient to parametrize the chiral field U as

$$U = \phi_0 + i\tau_a\phi_a, \quad (2)$$

with $a = 1$, 2, and 3 and the unitary constraint $(\phi_0)^2 + (\phi_a)^2 = 1$. Note that with this parametrization (2), ϕ_α ($\alpha = 0$, 1, 2, and 3) can be rephrased in terms of quark bilinear configurations as

$$\phi_0 \sim \bar{q}q, \quad \phi_a \sim \bar{q}i\gamma_5\tau_a q. \quad (3)$$

For later convenience, we further introduce the unnormalized fields $\bar{\phi}_\alpha$, which are related to the normalized fields ϕ_α through

$$\phi_\alpha = \frac{\bar{\phi}_\alpha}{\sqrt{\sum_{\beta=0}^3 \bar{\phi}_\beta\bar{\phi}_\beta}}. \quad (4)$$

For a crystal lattice with size $2L$, one can parametrize the unnormalized field $\bar{\phi}_\alpha$ in terms of the Fourier series as [13]

$$\begin{aligned}
\bar{\phi}_0(x,y,z) &= \sum_{a,b,c}\bar{\beta}_{abc}\cos(a\pi x/L)\cos(b\pi y/L)\cos(c\pi z/L),\\
\bar{\phi}_1(x,y,z) &= \sum_{h,k,l}\bar{\alpha}^{(1)}_{hkl}\sin(h\pi x/L)\cos(k\pi y/L)\cos(l\pi z/L),\\
\bar{\phi}_2(x,y,z) &= \sum_{h,k,l}\bar{\alpha}^{(2)}_{hkl}\cos(l\pi x/L)\sin(h\pi y/L)\cos(k\pi z/L),\\
\bar{\phi}_3(x,y,z) &= \sum_{h,k,l}\bar{\alpha}^{(3)}_{hkl}\cos(k\pi x/L)\cos(l\pi y/L)\sin(h\pi z/L),
\end{aligned} \quad (5)$$

where $\bar{\alpha}$ and $\bar{\beta}$ are free parameters that are determined by minimizing the energy of the system.

For a particular crystal lattice, the Fourier coefficients $\bar{\alpha}$ and $\bar{\beta}$ are not independent of each other. For example, the fcc crystal, which is used in the present work, possesses the following symmetry structure in position space and corresponding isospin space:

(i) reflection symmetry, in position space $(x,y,z) \leftrightarrow (-x,y,z)$ and in isospin space $(\phi_0,\phi_1,\phi_2,\phi_3) \leftrightarrow (\phi_0,-\phi_1,\phi_2,\phi_3)$;

(ii) threefold symmetry, in position space $(x,y,z) \leftrightarrow (z,x,y)$ and in isospin space $(\phi_0,\phi_1,\phi_2,\phi_3) \leftrightarrow (\phi_0,\phi_3,\phi_1,\phi_2)$;

(iii) fourfold symmetry, in position space $(x,y,z) \leftrightarrow (y,-x,z)$ and in isospin space $(\phi_0,\phi_1,\phi_2,\phi_3) \leftrightarrow (\phi_0,\phi_2,-\phi_1,\phi_3)$; and

(iv) translational symmetry, in position space $(x,y,z) \leftrightarrow (x+L,y+L,z)$ and in isospin space $(\phi_0,\phi_1,\phi_2,\phi_3) \leftrightarrow (\phi_0,-\phi_1,-\phi_2,\phi_3)$.

Hence the Fourier coefficients $\bar{\beta}_{abc}$ and $\bar{\alpha}^{(1,2,3)}_{hkl}$ have the following relations [13]:

(i) from threefold symmetry, $\bar{\beta}_{abc} = \bar{\beta}_{bca} = \bar{\beta}_{cab}$, $\bar{\alpha}^{(1)}_{hkl} = \bar{\alpha}^{(2)}_{hkl} = \bar{\alpha}^{(3)}_{hkl}$;

(ii) from fourfold symmetry, $\bar{\beta}_{abc} = \bar{\beta}_{acb} = \bar{\beta}_{cba} = \bar{\beta}_{bac}$ $\bar{\alpha}_{hkl} = \bar{\alpha}_{hlk}$; and

(iii) from translational symmetry, a, b, and c are all even numbers or odd numbers, and if h is even, then k and l are restricted to odd numbers, otherwise even numbers.

Note that there is a possibility that the constraint on the translational symmetry as above appears: From the translational symmetry, a, b, and c are all odd numbers, and h is odd, then k and l are restricted even numbers. This indicates that the Skyrmion crystal is invariant

under the following additional symmetry: In position space $(x, y, z) \leftrightarrow (x + L, y, z)$ and in isospin space $(\phi_0, \phi_1, \phi_2, \phi_3) \leftrightarrow (-\phi_0, -\phi_1, \phi_2, \phi_3)$. This configuration is nothing but the centered-cubic (cc) crystal.

This implies that the Skyrmion configuration is deformed from a fcc crystal to a cc crystal by changing the matter density, as will be seen in a later section.

B. Introducing the magnetic field in the Skyrmion crystal

Next, let us discuss how to introduce the magnetic field in the Skyrmion crystal model.

The magnetic field can be incorporated into the Skyrme model (1) by replacing the derivative operator with the gauge covariant one,

$$D_\mu U = \partial_\mu U - ieA_\mu[Q_E, U], \tag{6}$$

where e is the electromagnetic coupling constant and $Q_E = \frac{1}{6} + \frac{1}{2}\tau_3$ is the electric charge matrix, with τ_3 being the third component of the Pauli matrix. In the present work, we consider a constant magnetic field B along the z direction. Then, taking into account the residual $O(2)$ symmetry for the x-y plane perpendicular to the B axis, we choose the following symmetric gauge:[2]

$$A_\mu = -\tfrac{1}{2}By\delta_\mu{}^1 + \tfrac{1}{2}Bx\delta_\mu{}^2. \tag{7}$$

In terms of the parametrization (2), we can write the covariant derivative operator as

$$D_\mu U = \partial_\mu\phi_0 + iD_\mu\phi_1\tau_1 + iD_\mu\phi_2\tau_2 + i\partial_\mu\phi_3\tau_3, \tag{8}$$

where $D_\mu\phi_1 = \partial_\mu\phi_1 - eA_\mu\phi_2$ and $D_\mu\phi_2 = \partial_\mu\phi_2 + eA_\mu\phi_1$.

In the Skyrmion crystal model with the electromagnetic charge turned on, a covariant derivative operator such as $D_x\phi_1$ should be discretized to hold the translational invariance in the x-y plane. Then, with the help of the Fourier transformation, $y\bar{\phi}_2(x, y, z)$ goes as follows:

$$\begin{aligned}
y\bar{\phi}_2(x, y, z) &= y\int_{-\infty}^{\infty}\frac{dp_x}{(2\pi)}\int_{-\infty}^{\infty}\frac{dp_y}{(2\pi)}\int_{-\infty}^{\infty}\frac{dp_z}{(2\pi)}\bar{\phi}_2(p_x, p_y, p_z)e^{i\vec{p}\cdot\vec{x}} \\
&= \int_0^{\infty}\frac{dp_x}{(2\pi)}\int_0^{\infty}\frac{dp_y}{(2\pi)}\int_0^{\infty}\frac{dp_z}{(2\pi)}\bar{\phi}_2(p_x, p_y, p_z)8i\cos(p_x x)\big[-\partial_{p_y}\cos(p_y y)\big]\cos(p_z z) \\
&\xrightarrow{\text{discretization}} -\sum_{h,k,l}\bar{\alpha}^{(2)}_{h,k,l}\cos(l\pi x/L)\frac{\cos\{(h+2)\pi y/L\} - \cos(h\pi y/L)}{2\pi/L}\cos(k\pi z/L) \\
&\equiv [y\bar{\phi}_2]_{\text{disc}}(x, y, z),
\end{aligned} \tag{9}$$

where the second equality was obtained by the reflection symmetry. One can easily check the translational covariance for $[y\bar{\phi}_2]_{\text{disc}}(x, y, z)$. After making the translation $(x, y, z) \to (x + L, y + L, z)$, for instance, $[y\bar{\phi}_2]_{\text{disc}}(x, y, z)$ obviously transforms to

$$[y\bar{\phi}_2]_{\text{disc}}(x, y, z) \to -[y\bar{\phi}_2]_{\text{disc}}(x, y, z). \tag{10}$$

Similarly, the translational covariance holds in the following discretized forms:

$$\begin{aligned}
[x\bar{\phi}_1]_{\text{disc}}(x, y, z) &= -\sum_{h,k,l}\bar{\alpha}_{h,k,l}\frac{\cos\{(h+2)\pi x/L\} - \cos(h\pi x/L)}{2\pi/L}\cos(k\pi y/L)\cos(l\pi z/L), \\
[y\bar{\phi}_1]_{\text{disc}}(x, y, z) &= \sum_{h,k,l}\bar{\alpha}_{h,k,l}\sin(h\pi x/L)\frac{\sin\{(k+2)\pi y/L\} - \sin(k\pi y/L)}{2\pi/L}\cos(l\pi z/L), \\
[x\bar{\phi}_2]_{\text{disc}}(x, y, z) &= \sum_{h,k,l}\bar{\alpha}_{h,k,l}\frac{\sin\{(l+2)\pi x/L\} - \sin(l\pi x/L)}{2\pi/L}\sin(h\pi y/L)\cos(k\pi z/L).
\end{aligned} \tag{11}$$

Let us check whether the other symmetries in the fcc crystal are kept in the presence of a magnetic field. For instance, the covariant derivative of ϕ_1 is transformed as

$$[D_i\phi_1]_{\text{disc}}(x, y, z) \xrightarrow{\text{reflection:}(x,y,z)\to(-x,y,z)} \begin{cases} (i = x) & [D_x\phi_1]_{\text{disc}}(x, y, z), \\ (i = y) & -[D_y\phi_1]_{\text{disc}}(x, y, z), \\ (i = z) & -[D_z\phi_1]_{\text{disc}}(x, y, z), \end{cases}$$

$$[D_i\phi_1]_{\text{disc}}(x, y, z) \xrightarrow{\text{translation:}(x,y,z)\to(x+L,y+L,z)} -[D_i\phi_1]_{\text{disc}}(x, y, z),$$

[2]Because we model the nuclear matter by the Skyrmion crystal, it is necessary to choose the symmetric gauge that keeps the $O(2)$ symmetry appropriate to form the crystal. This kind of gauge dependence can also be seen in the ladder approximations, where, as is well known, QCD observables are modeled and computed with some specific gauge choice to be consistent with the associated chiral symmetry (e.g., see Refs. [22–26]).

$$
\begin{aligned}
[D_i\phi_1]_{\rm disc}(x,y,z) &\xrightarrow{\text{twofold for } z \text{ axis: } (x,y,z)\to(y,-x,z)} \begin{cases} (i=x)\ \ (\partial_y\phi_2 + eA_y\phi_1)_{\rm disc}(x,y,z), \\ (i=y)\ \ -(\partial_x\phi_2 + eA_x\phi_1)_{\rm disc}(x,y,z), \\ (i=z)\ \ [D_z\phi_2]_{\rm disc}(x,y,z), \end{cases} \\
[D_i\phi_1]_{\rm disc}(x,y,z) &\xrightarrow{\text{twofold for } x \text{ axis: } (x,y,z)\to(x,z,-y)} \begin{cases} (i=x)\ \ (\partial_x\phi_1 - eA_x\phi_3)_{\rm disc}(x,y,z), \\ (i=y)\ \ (\partial_z\phi_1 - eA_z\phi_3)_{\rm disc}(x,y,z), \\ (i=z)\ \ -(\partial_y\phi_1 - eA_y\phi_3)_{\rm disc}(x,y,z), \end{cases} \\
[D_i\phi_1]_{\rm disc}(x,y,z) &\xrightarrow{\text{threefold: } (x,y,z)\to(z,x,y)} \begin{cases} (i=x)\ \ (\partial_z\phi_3 - eA_z\phi_1)_{\rm disc}(x,y,z), \\ (i=y)\ \ (\partial_x\phi_3 - eA_x\phi_1)_{\rm disc}(x,y,z), \\ (i=z)\ \ (\partial_y\phi_3 - eA_y\phi_1)_{\rm disc}(x,y,z). \end{cases}
\end{aligned} \tag{12}
$$

One can see easily that, as naively expected, the two-fold symmetry for $x(y)$ axis and the three-fold symmetry are explicitly broken by the magnetic field in the z direction.

C. Baryon-number density of a Skyrmion crystal in a magnetic field

In the presence of a magnetic field, the baryon-number current is evaluated as [27]

$$j_B^\mu = j_W^\mu + \mathcal{J}_{eB}^\mu, \tag{13}$$

where

$$
\begin{aligned}
j_W^\mu &= \frac{1}{24\pi^2}\epsilon^{\mu\nu\rho\sigma}{\rm tr}[(\partial_\nu U\cdot U^\dagger)(\partial_\rho U\cdot U^\dagger)(\partial_\sigma U\cdot U^\dagger)], \\
\mathcal{J}_{eB}^\mu &= \frac{1}{16\pi^2}\epsilon^{\mu\nu\rho\sigma}{\rm tr}[ie(\partial_\nu A_\rho)Q_E(\partial_\sigma U\cdot U^\dagger + U^\dagger\partial_\sigma U) \\
&\quad + ieA_\nu Q_E(\partial_\rho U\partial_\sigma U^\dagger - \partial_\rho U^\dagger\partial_\sigma U)],
\end{aligned} \tag{14}
$$

in which j_W^μ corresponds to the winding-number current and $\mathcal{J}_{eB}^\mu$ is the induced current by the magnetic field. Under the symmetric gauge, the time component of the induced current takes the form

$$
\begin{aligned}
\mathcal{J}_{eB}^0 &= -\frac{eB}{4\pi^2}[(\partial_z\phi_3)\phi_0 - (\partial_z\phi_0)\phi_3] \\
&\quad + \frac{eB}{8\pi^2}\big(\{[y\partial_y\phi_3]_{\rm disc}(\partial_z\phi_0) - [y\partial_y\phi_0]_{\rm disc}(\partial_z\phi_3)\} \\
&\quad - \{(\partial_z\phi_3)[x\partial_x\phi_0]_{\rm disc} - (\partial_z\phi_0)[x\partial_x\phi_3]_{\rm disc}\}\big).
\end{aligned} \tag{15}
$$

Explicit expressions of the discretized form involving a derivative as above are given in the Appendix. Then the total baryon-number density $\rho_B(x,y,z)$ is written as

$$
\begin{aligned}
\rho_B(x,y,z) &= j_W^0(x,y,z) + \mathcal{J}_{eB}^0(x,y,z) \\
&\equiv \rho_W(x,y,z) + \tilde{\rho}_{eB}(x,y,z),
\end{aligned} \tag{16}
$$

where $\rho_W(z,y,z)$ is the winding-number density and $\tilde{\rho}_{eB}(x,y,z)$ is the baryon-number density induced by a magnetic field. The baryon number is obtained by performing the spacial integration $N_B = \int_{\rm cube} d^3x\rho_B$. As in the case without a magnetic field, the baryon number in a single fcc crystal is normalized as

$$N_B = \int_{\rm cube} d^3x\rho_B = 4, \tag{17}$$

because $\int_{\rm cube} d^3x\tilde{\rho}_{eB} = 0$.[3]

III. MAGNETIC FIELD EFFECT IN A SKYRMION CRYSTAL

With the above setup, we are now ready to numerically simulate the magnetic effect on the nuclear matter. For this purpose, we take the following typical values[4] [29]

$$f_\pi = 92.4\ {\rm MeV}, \quad g = 5.93. \tag{18}$$

A. Per-baryon energy E/N_B

The per-baryon energy is given by

$$E/N_B = \frac{1}{4}\int_{\rm cube} d^3x\mathcal{H}_{\rm Skyr}^B, \tag{19}$$

with $\mathcal{H}_{\rm Skyr}^B$ being the static Skyrmion energy in the presence of the external magnetic field introduced as above. In Eq. (19), the per-baryon energy is given as a function of the Fourier coefficients $\bar{\beta}_{abc}$ and $\bar{\alpha}_{hkl}^{(i)}$, the crystal size L, and the magnetic field strength eB. For the chosen crystal size L and the magnetic strength eB, we use the Fourier coefficients as variational parameters to minimize the per-baryon energy. In this way, the per-baryon energy can be calculated as a function of the crystal size L and the magnetic field strength eB.

In Fig. 1 we plot the per-baryon energy as a function of the crystal size with typical values for the magnetic field strengths

[3] By using Eq. (5) and the symmetry relations, one can derive

$$
\begin{aligned}
&\int_{\rm cube} d^3x\,(\partial_z\phi_3)\phi_0 = \int_{\rm cube} d^3x\,\phi_3\partial_z\phi_0 = 0, \\
&\int_{\rm cube} d^3x\,[y(\partial_y\phi_3)]_{\rm disc}(\partial_z\phi_0) = \int_{\rm cube} d^3x\,[y(\partial_y\phi_0)]_{\rm disc}(\partial_z\phi_3) = 0, \\
&\int_{\rm cube} d^3x\,[x(\partial_x\phi_3)]_{\rm disc}(\partial_z\phi_0) = \int_{\rm cube} d^3x\,[x(\partial_x\phi_0)]_{\rm disc}(\partial_z\phi_3) = 0.
\end{aligned}
$$

Here we used the same Fourier expansion form for ϕ_α as that for $\bar{\phi}_\alpha$, as in Eq. (5). Thus one can find $\int_{\rm cube}\mathcal{J}_B^0(eB) = 0$; hence the baryon number is conserved under a magnetic field.

[4] We determine the Skyrme parameter g by integrating out the vector mesons from the chiral effective theory of vector mesons based on the hidden local symmetry approach (see, e.g., Ref. [28]). In such a way, the Skyrme parameter can be related to the ρ-π-π coupling through $g = g_{\rho\pi\pi} = m_\rho/(\sqrt{2}f_\pi) \simeq 5.93$ [29].

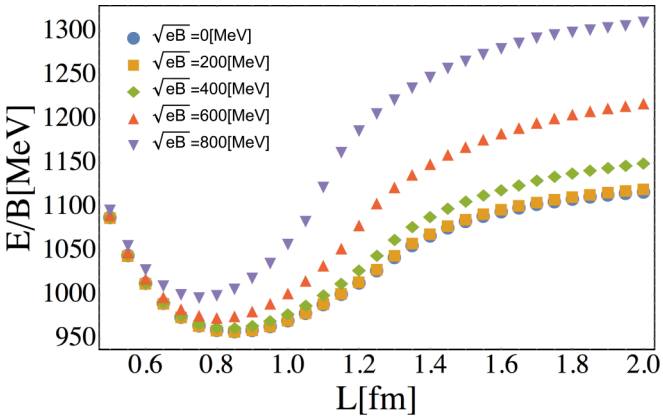

FIG. 1. The per-baryon energy in the magnetic field as a function of the crystal size L.

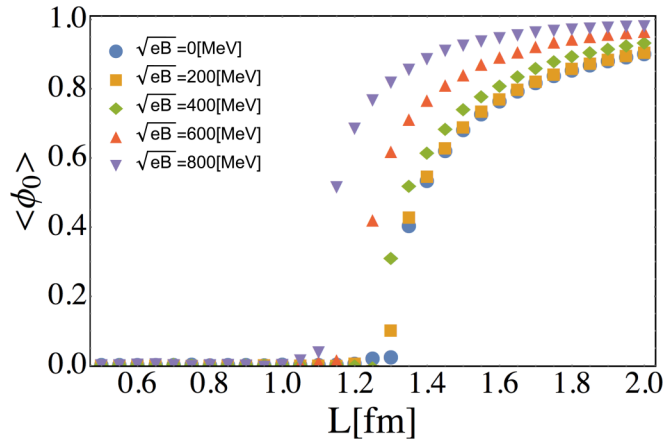

FIG. 2. $\langle\phi_0\rangle$, in the magnetic field, as a function of the crystal size L.

fixed. Note first that the bottommost curve in Fig. 1 precisely reproduces the crystal-size dependence of the per-baryon energy in Ref. [29] without the magnetic field ($eB=0$), which manifests a check of our numeric code. From Fig. 1 we see that, for a fixed crystal size L, the per-baryon energy monotonically increases as the magnetic field increases. In the low-density region (large crystal size L), this tendency can be compared with the result obtained in Ref. [27] for an isolated Skyrmion (not in the Skyrmion crystal). One can also see an interesting discrepancy in comparison with the reference: the Skyrmion energy analyzed in Ref. [27] has a minimum with respect to eB, due to a destructive interference between the $\mathcal{O}(eB)$ and $\mathcal{O}((eB)^2)$ terms in the per-baryon energy functional. On the contrary, this is not the case for our present work. In the Skyrmion crystal approach, the $\mathcal{O}(eB)$ terms disappear when the per-baryon energy functional is integrated over the volume of the crystal, which is due to the crystal structure symmetry,[5] so that only $\mathcal{O}((eB)^2)$ terms survive. This observation is supported from the magnetic field dependence of the per-baryon energy at low density in Fig. 1.

Unlike the low-density region, in the high-density region (small L), the per-baryon energy hardly gets affected by the magnetic field. To understand this tendency we rescale the position space by the crystal size $x=x'/L$ and rewrite the covariant derivative as $D_x\phi_1=(\partial_{x'}\phi_1+\frac{eBL^2}{2}y'\phi_2)/L$. This shows that the magnetic effect becomes weaker when the crystal size is reduced.[6]

[5]For example, the Lagrangian has an $\mathcal{O}(eB)$ term such as $eA_i\phi_2\partial_i\phi_1=eA_x\phi_2\partial_x\phi_1+eA_y\phi_2\partial_y\phi_1$. By using Eq. (5) and symmetry relations, one finds

$$\int d^3x eA_x\phi_2\partial_x\phi_1=-\frac{eB}{2}\int d^3x\,[y\phi_2]_{\rm disc}\partial_x\phi_1=0.$$

Also, the integration for $eA_y\phi_2\partial_y\phi_1$ becomes 0 in a way similar to that of footnote 3.

[6]Note also from Fig. 1 that, as the magnetic field increases, the per-baryon energy gets enhanced for every crystal size L. This could be related to the generation of the magnetic moment for the Skyrmion, when the Skyrmion is quantized to be endowed with spin and isospin quantum numbers.

B. Topology transition in baryonic matter and its related phenomena: Inhomogeneity of the chiral condensate

In the Skyrmion approach to nuclear matter, a novel phenomenon, which is not observed in other approaches, is the so-called Skyrmion to half-Skyrmion transition, where the fcc crystal with one Skyrmion (baryon number 1) at each vertex factorizes to the cc crystal with a half-skymrion (having baryon number 1/2) at each crystal vertex [30,31]. (The presence of the half-Skyrmion is a robust prediction that has arisen along the maximal (discrete) symmetry [32].) We will call this phenomenon "topological transition in the baryonic matter." The space-averaged value $\langle\phi_0\rangle=\frac{1}{(2L)^3}\int_0^{2L}d^3x\phi_0$ vanishes at some critical crystal size, which signals the topology transition, as we will see through the baryon-number density later. Hereafter we refer to the Skyrmion crystal of the fcc crystal as the Skyrmion phase and the cc crystal of the half-Skyrmion as the half-Skyrmion phase.

Figure 2 shows the magnetic dependence of $\langle\phi_0\rangle$, the vanishing of which signals the topology transition in the baryonic matter. Again, without a magnetic field ($\sqrt{eB}=0$), the critical point at $\langle\phi_0\rangle=0$ agrees with that obtained in Ref. [29] (see the bottommost curve in the figure). From Fig. 2, one can see that as the magnetic field increases, the phase transition point is shifted to a high-density region and the value of the order parameter $\langle\phi_0\rangle$ gets larger. Moreover, this enhancement can be rephrased as a magnetic catalysis for the chiral condensate, because ϕ_0 can be associated with $\bar{q}q$ [see Eq. (3)].

In addition to the topology transition in the baryonic matter, the spatial distribution of ϕ_0 can actually be thought of as an inhomogeneous chiral condensate with ϕ_a as its chiral partner. We plot in Figs. 3 and 4 the magnetic dependence of the distributions of $\phi_0(x,y,z)$ and $\phi_1(x,y,z)$ at $L=2.0$ fm (in the Skyrmion phase). Figures 3(a) and 4(a) show the inhomogeneities of ϕ_0 and ϕ_1 in the absence of the magnetic field, where the inhomogeneous configurations take a form like a "pulse" for $\phi_0(\sim\bar{q}q)$ and a "wave" for $\phi_1(\sim\bar{q}i\gamma_5\tau^1q)$. Figures 3(a) and 4(a) agree with the analysis in Ref. [33]. Turning on the magnetic field [panels (b) and (c) in

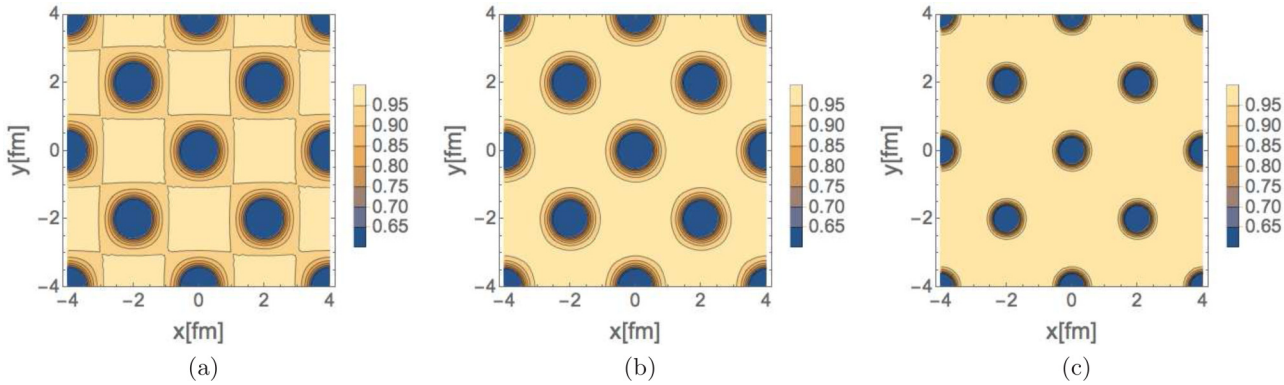

FIG. 3. The distributions of $\phi_0(x, y, 0)$ at $L = 2.0\,\mathrm{fm}$ (in the Skyrmion phase) for $\sqrt{eB} = 0$ (a), $\sqrt{eB} = 400\,\mathrm{MeV}$ (b), and $\sqrt{eB} = 800\,\mathrm{MeV}$ (c).

Figs. 3 and 4], one notices a striking phenomenon: as eB gets bigger, the ϕ_0 and ϕ_1 inhomogeneities tend to be drastically localized at the vertices of the crystal (keeping each shape of the "pulselike" and "wavelike" forms). Because of the dramatic localization, the density $n_{1/2}$ at which the Skyrmion matter transits to the half-Skyrmion matter becomes larger. This novel tendency can more easily be captured by zooming in the $y = z = 0$ plane, as depicted in Fig. 5. Similar observations, regarding the deformation of inhomogeneities for the chiral condensate by magnetic effects, have been made in different models [18–21].

We next show in Figs. 6 and 7 the magnetic dependence on the distributions of $\phi_0(x, y, z)$ and $\phi_1(x, y, z)$ in the half-Skyrmion phase at $L = 1.0\,\mathrm{fm}$. Figures 6(a) and 7(a) show the inhomogeneities of ϕ_0 and ϕ_1 without the magnetic field. The results seen in Figs. 6(a) and 7(a) are, again, consistent with the analysis in Ref. [33]. When the magnetic field is turned on [panels (b) and (c) in Figs. 6 and 7], one can see that the ϕ_0 and ϕ_1 inhomogeneities are hardly affected by the strength of eB. This is in contrast to the situation in the Skyrmion phase. This can also be illustrated by zooming in the $y = z = 0$ plane in Fig. 8.

C. Pion decay constant

We next turn to the order parameter of the chiral symmetry breaking, f_π, in the Skyrmion crystal with a magnetic effect. We introduce the fluctuating pion field through

$$U = \breve{u}\bar{U}\breve{u},$$
$$\breve{u} = \exp[i\pi^a\tau^a/(2f_\pi)], \tag{20}$$

where $\bar{U}$ is the background Skyrmion field and π^a describes the fluctuating pion field. Thus, the medium-modified pion-decay constant, f_π^*, is obtained as [13]

$$\frac{f_\pi^*}{f_\pi} = \sqrt{1 - \frac{2}{3}\left(1 - \langle\phi_0^2\rangle\right)}. \tag{21}$$

In Fig. 9 we plot f_π^*/f_π as a function of the crystal size of L with the magnetic field varied. The density dependence at $\sqrt{eB} = 0$ agrees with the result of Ref. [13].[7] Furthermore, in the presence of the magnetic field, the magnitude of the

[7] f_π^*/f_π can be vanishing at the chiral-phase transition point if one takes into account a chiral-singlet ("dilaton") effect as discussed in Ref. [34].

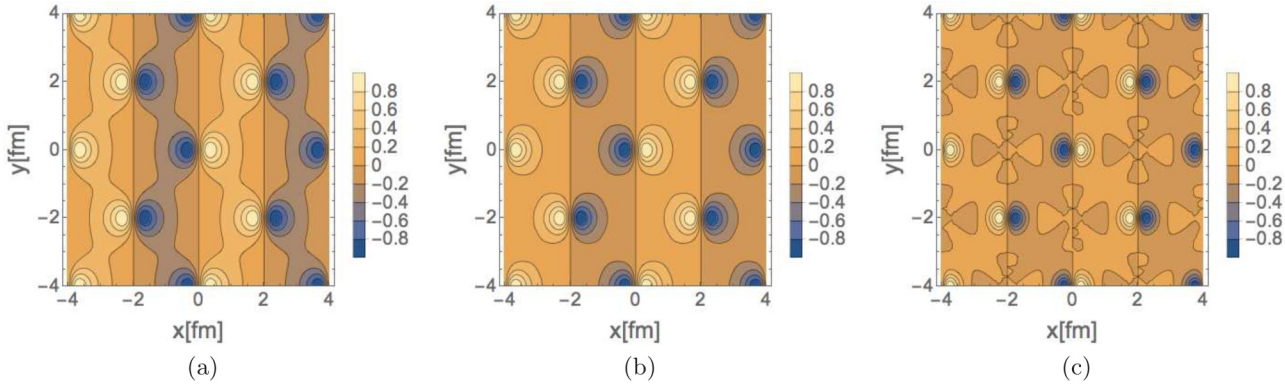

FIG. 4. The distributions of $\phi_1(x, y, 0)$ at $L = 2.0\,\mathrm{fm}$ (in the Skyrmion phase) for $\sqrt{eB} = 0$ (a), $\sqrt{eB} = 400\,\mathrm{MeV}$ (b), and $\sqrt{eB} = 800\,\mathrm{MeV}$ (c).

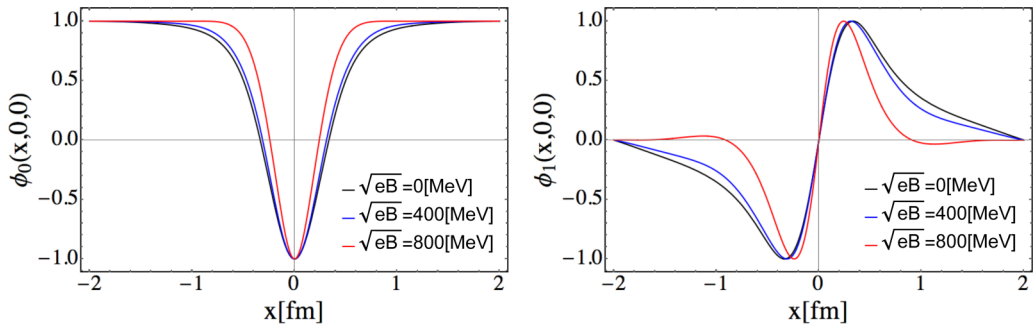

FIG. 5. The distributions of $\phi_0(x, 0, 0)$ (a) and $\phi_1(x, 0, 0)$ (b) at $L = 2.0$ fm (in the Skyrmion phase) with $\sqrt{eB}$ varied.

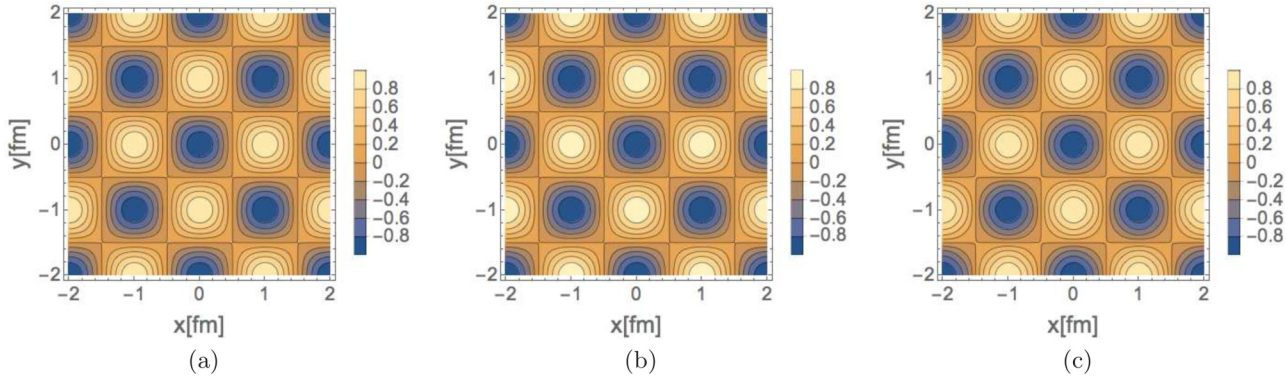

FIG. 6. The distributions of $\phi_0(x, y, 0)$ at $L = 1.0$ fm (in the half-Skyrmion phase) for $\sqrt{eB} = 0$ (a), $\sqrt{eB} = 400$ MeV (b), and $\sqrt{eB} = 800$ MeV (c).

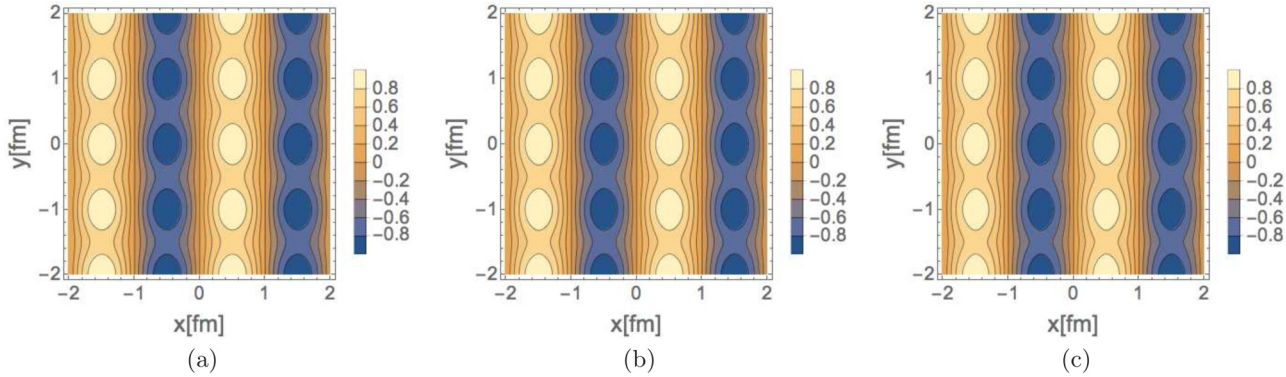

FIG. 7. The distributions of $\phi_1(x, y, 0)$ at $L = 1.0$ fm (in the half-Skyrmion phase) for $\sqrt{eB} = 0$ (a), $\sqrt{eB} = 400$ MeV (b), and $\sqrt{eB} = 800$ MeV (c).

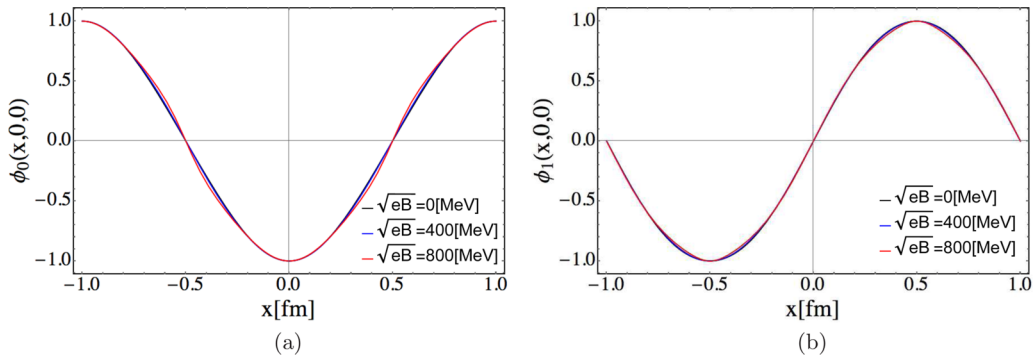

FIG. 8. The distributions of $\phi_0(x, 0, 0)$ (a) and $\phi_1(x, 0, 0)$ (b) at $L = 1.0$ fm (in the half-Skyrmion phase) with $\sqrt{eB}$ varied.

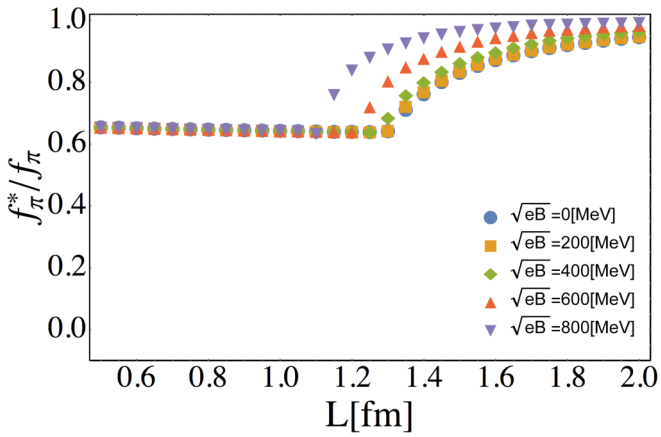

FIG. 9. The pion-decay constant normalized to the matter-free value, f_π^*/f_π, as a function of the crystal size L with a different choice of the magnetic field.

chiral symmetry breaking gets larger when the strength of the magnetic field is increased. Again this implies the magnetic catalysis for the chiral symmetry breaking, as discussed in Ref. [35].

D. Deformation of the Skyrmion configuration

We finally in this section discuss the deformation of the Skyrmion configuration and the baryon shape in the presence of a magnetic field.

In the Skyrmion crystal approach the Skyrmion configuration can be extracted by plotting the position dependence of the the baryon-number density distribution functions in Eq. (16). From Eq. (16) one can check that the winding-number density $\rho_W(x, y, z)$ keeps the crystal symmetries for the FCC and CC structures in the presence of a magnetic field. However, the induced baryon-number density $\tilde{\rho}_{eB}$ does not have this feature. This implies that the Skyrmion configurations in both phases would be significantly deformed by the presence of the magnetic field.

In Figs. 10 and 11, we plot the Skyrmion configurations in the Skyrmion phase. First, it is interesting to note that even for a large magnetic field eB, the fcc crystal structure essentially holds (see, in particular, Fig. 11 for $\sqrt{eB} = 800\,\mathrm{MeV}$). For the single baryon's shape (corresponding to higher-intense objects in Figs. 10 and 11), one also finds that it is deformed to be an elliptic form by the magnetic field. The deformation of this kind has also been found in the isolated Skyrmion analysis in matter-free space [27].

We now move on to the half-Skyrmion phase. We make plots of the half-Skyrmion configurations in Figs. 12 and 13. One can immediately see that the half-Skyrmion configuration is dramatically deformed by the presence of a magnetic field and the magnetic effect not only breaks the cc form, but also makes a multiple-peak structure (Fig. 13). Those nontrivial deformations in the half-Skyrmion phase would be indirect probes for the presence of inhomogeneous chiral condensate shown in Fig. 7.

IV. SUMMARY

In this article, we analyzed magnetic field effects on nuclear matter based on the Skyrmion crystal approach for the first time. As was listed in the Introduction, several interesting phenomena have been found which would be relevant to the equation of state of compact stars. We will not repeat them here.

In closing, we shall make a few comments on what we have found and the related prospect on its phenomenological implications. As is well known, the Skyrmion crystal model is not appropriate to simulate nuclear matter in a low-density region such as a region below the normal nuclear density where the nuclear matter is expected to be made of liquid drops or hadron gas. In contrast, in a high-density region our crystalline description for nuclear matter could be valid, because in such a region nucleons are nearly compressed at a certain fixed position, being treated as static objects, and hence can be qualitatively well described by solitons in a large N_c limit.

Though it might quantitatively be somewhat away from the realistic situation for nuclear matter, magnetic effects on the phase transition, such as the magnetic catalysis, would qualitatively involve curious enough aspects for high dense

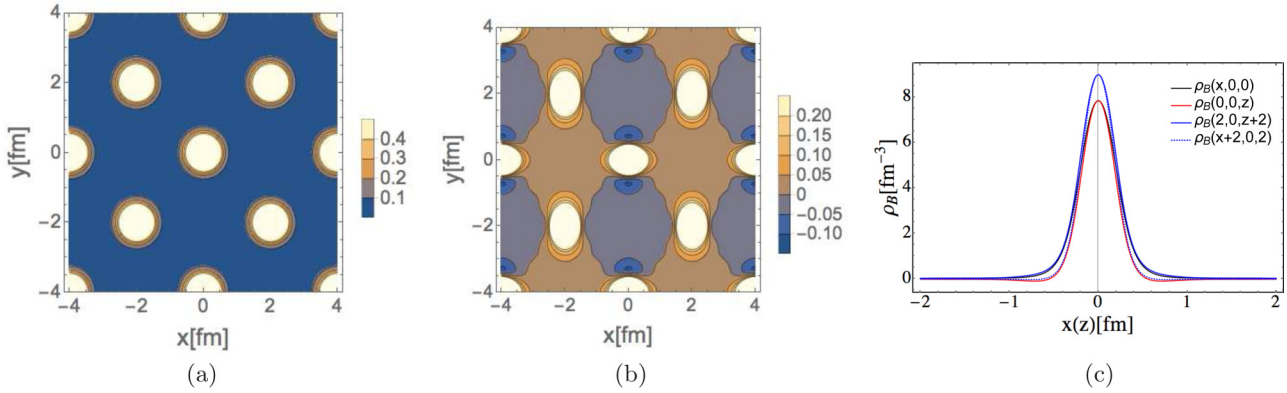

FIG. 10. The Skyrmion configurations at $\sqrt{eB} = 400\,\mathrm{MeV}$ and $L = 2.0\,\mathrm{fm}$ (in the Skyrmion phase). (a) The density contour plot on the x-y plane. (b) The density contour plot on the x-z plane. (c) The distribution along the x axis or the z axis including the size rescaled by $L = 2.0\,\mathrm{fm}$.

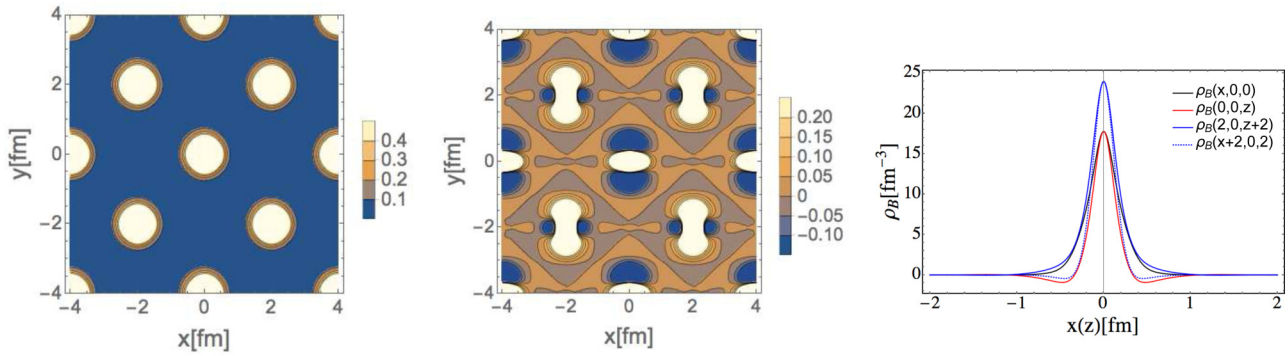

(a) (b) (c)

FIG. 11. The Skyrmion configurations at $\sqrt{eB} = 800\,\text{MeV}$ and $L = 2.0\,\text{fm}$ (in the Skyrmion phase). (a) The density contour plot on the x-y plane. (b) The density contour plot on the x-z plane. (c) The distribution along the x axis or the z axis including the size rescaled by $L = 2.0\,\text{fm}$.

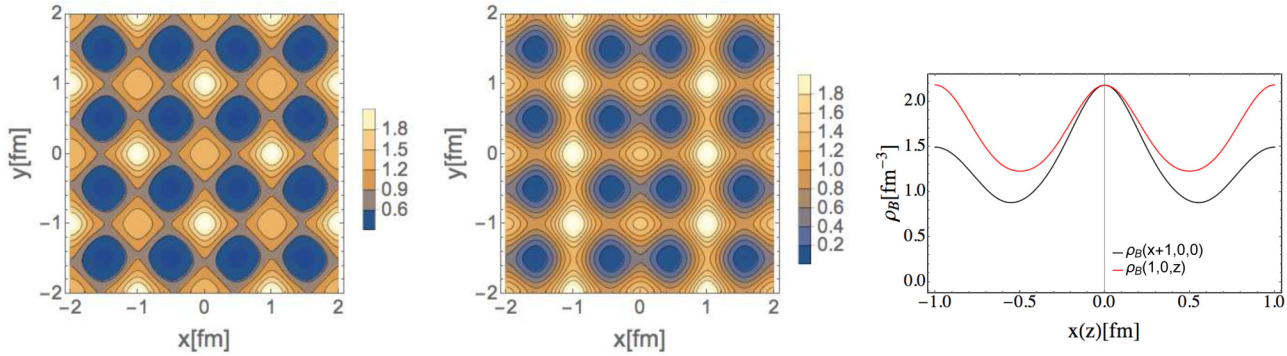

(a) (b) (c)

FIG. 12. The Skyrmion configurations at $\sqrt{eB} = 400\,\text{MeV}$ and $L = 1.0\,\text{fm}$ (in the half-Skyrmion phase). (a) The density contour plot on the x-y plane. (b) The density contour plot on the x-z plane. (c) The distribution along the x axis or the z axis including the size of the shift by $L = 1.0\,\text{fm}$.

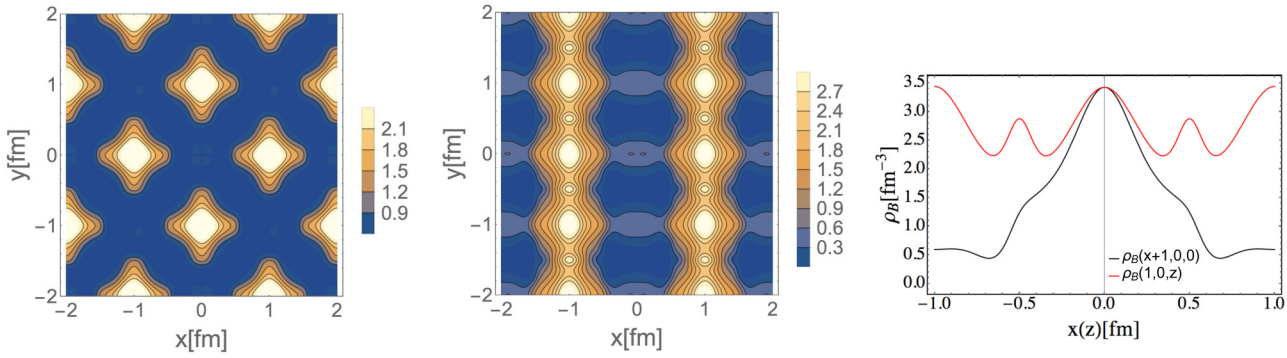

(a) (b) (c)

FIG. 13. The Skyrmion configurations at $\sqrt{eB} = 800\,\text{MeV}$ and $L = 1.0\,\text{fm}$ (in half-Skyrmion phase). (a) The density contour plot on x-y plane. (b) The density contour plot on x-z plane. (c) The distribution along the x axis or the z axis including the size of the shift by $L = 1.0\,\text{fm}$.

matter physics in a strong magnetic field. A strong magnetic field might be generated in the core of neutron stars or magnetars in correlation with a chiral dynamics, as was discussed in Refs. [36,37]. In that case, the remnant of the topology transition in the baryonic matter including the characteristic magnetic effect may be incorporated into the equation of state for the neutron stars, as in Refs. [38–40], to simulate the compact star properties, which might be observed in the near future.

ACKNOWLEDGMENTS

M.K. would like to thank the support from Jilin University where the early stage of this work was done. The work of M.K. is supported in part by JSPS Grant-in-Aid for JSPS Research Fellow No. 18J15329. Y.L.M. was supported in part by the National Science Foundation of China (NSFC) under Grants No. 11475071 and No. 11747308 and by the Seeds Funding of Jilin University. The work of S.M. was supported in part by JSPS Grant-in-Aid for Young Scientists (B) No. 15K17645.

APPENDIX: DISCRETIZATION OF $x\partial_i\phi_a$

In this appendix, we present the method for discretizing the quantity including a derivative. For example, we consider the quantity $x\partial_x\phi_3$:

$$[x\partial_x\phi_3]_{\rm disc} = \frac{[x\partial_x\bar{\phi}_3]_{\rm disc}}{\sqrt{\bar{\phi}_a\bar{\phi}_a}} - \frac{(\bar{\phi}_b[x\partial_x\bar{\phi}_b]_{\rm disc})\bar{\phi}_3}{(\bar{\phi}_a\bar{\phi}_a)^{3/2}}. \quad \text{(A1)}$$

We make discretizations for the square bracket parts denoted as $[\ \ ]_{\rm disc}$. The $[x\partial_x\bar{\phi}_0]_{\rm disc}$ part is computed as

$$\begin{aligned} x\partial_x\bar{\phi}_0(x,y,z) &= x\partial_x\int_0^\infty\frac{dp_x}{(2\pi)}\int_0^\infty\frac{dp_y}{(2\pi)}\int_0^\infty\frac{dp_z}{(2\pi)}\bar{\phi}_0(\mathbf{p})8\cos(p_x x)\cos(p_y y)\cos(p_z z) \\ &= \int_0^\infty\frac{dp_x}{(2\pi)}\int_0^\infty\frac{dp_y}{(2\pi)}\int_0^\infty\frac{dp_z}{(2\pi)}\bar{\phi}_0(\mathbf{p})8[p_x\partial_{p_x}\cos(p_x x)]\cos(p_y y)\cos(p_z z) \\ &\xrightarrow{\text{discretization}} \sum_{a,b,c}\bar{\beta}_{abc}\frac{a\pi}{L}\frac{\cos\{(a+2)\pi x/L\}-\cos(a\pi x/L)}{2\pi/L}\cos(b\pi y/L)\cos(c\pi z/L) \\ &\equiv [x\partial_x\bar{\phi}_0]_{\rm disc}(x,y,z). \end{aligned} \quad \text{(A2)}$$

Similarly, for other terms, we have

$$\begin{aligned} [x\partial_x\bar{\phi}_1]_{\rm disc} &= \sum_{h,k,l}\bar{\alpha}^{(1)}_{hkl}\frac{h\pi}{L}\frac{\sin\{(h+2)\pi x/L\}-\sin(h\pi x/L)}{2\pi/L}\cos(k\pi y/L)\cos(l\pi z/L), \\ [x\partial_x\bar{\phi}_2]_{\rm disc} &= \sum_{h,k,l}\bar{\alpha}^{(2)}_{hkl}\frac{l\pi}{L}\frac{\cos\{(l+2)\pi x/L\}-\cos(l\pi x/L)}{2\pi/L}\sin(h\pi y/L)\cos(k\pi z/L), \\ [x\partial_x\bar{\phi}_3]_{\rm disc} &= \sum_{h,k,l}\bar{\alpha}^{(3)}_{hkl}\frac{k\pi}{L}\frac{\cos\{(k+2)\pi x/L\}-\cos(k\pi x/L)}{2\pi/L}\cos(l\pi y/L)\sin(h\pi z/L). \end{aligned} \quad \text{(A3)}$$

Putting those terms into the right-hand side of Eq. (A1), we thus obtain the discretized form of $x\partial_x\phi_3$.

[1] J. O. Andersen, W. R. Naylor, and A. Tranberg, Phase diagram of QCD in a magnetic field: A review, Rev. Mod. Phys. **88**, 025001 (2016).
[2] I. A. Shushpanov and A. V. Smilga, Quark condensate in a magnetic field, Phys. Lett. B **402**, 351 (1997).
[3] N. O. Agasian and I. A. Shushpanov, Gell-Mann-Oakes-Renner relation in a magnetic field at finite temperature, J. High Energy Phys. 10 (2001) 006.
[4] E. S. Werbos, The chiral condensate in a constant electromagnetic field at $\mathcal{O}(p^6)$, Phys. Rev. C **77**, 065202 (2008).
[5] J. O. Andersen, Thermal pions in a magnetic background, Phys. Rev. D **86**, 025020 (2012).
[6] D. P. Menezes, M. B. Pinto, S. S. Avancini, A. P. Martínez, and C. Providência, Quark matter under strong magnetic fields in the Nambu-Jona-Lasinio Model, Phys. Rev. C **79**, 035807 (2009).
[7] T. Inagaki, D. Kimura, and T. Murata, Four fermion interaction model in a constant magnetic field at finite temperature and chemical potential, Prog. Theor. Phys. **111**, 371 (2004).
[8] J. K. Boomsma and D. Boer, The Influence of strong magnetic fields and instantons on the phase structure of the two-flavor NJL model, Phys. Rev. D **81**, 074005 (2010).
[9] L. Yu, J. Van Doorsselaere, and M. Huang, Inverse magnetic catalysis in the three-flavor NJL model with axial-vector interaction, Phys. Rev. D **91**, 074011 (2015).
[10] H. Liu, X. Wang, L. Yu, and M. Huang, Neutral and charged scalar mesons, pseudoscalar mesons, and diquarks in magnetic fields, Phys. Rev. D **97**, 076008 (2018).
[11] T. H. R. Skyrme, A unified field theory of mesons and baryons, Nucl. Phys. **31**, 556 (1962).
[12] I. R. Klebanov, Nuclear matter in the skyrme model, Nucl. Phys. B **262**, 133 (1985).

[13] H. J. Lee, B. Y. Park, D. P. Min, M. Rho, and V. Vento, A unified approach to high density: Pion fluctuations in skyrmion matter, Nucl. Phys. A **723**, 427 (2003).
[14] H. J. Lee, B. Y. Park, M. Rho, and V. Vento, The pion velocity in dense skyrmion matter, Nucl. Phys. A **741**, 161 (2004).
[15] Y. L. Ma, M. Harada, H. K. Lee, Y. Oh, B. Y. Park, and M. Rho, Dense baryonic matter in the hidden local symmetry approach: Half-skyrmions and nucleon mass, Phys. Rev. D **88**, 014016, (2013); **88**, 079904(E) (2013).
[16] Y. L. Ma, M. Harada, H. K. Lee, Y. Oh, B. Y. Park, and M. Rho, Dense baryonic matter in conformally-compensated hidden local symmetry: Vector manifestation and chiral symmetry restoration, Phys. Rev. D **90**, 034015 (2014).
[17] Y. L. Ma and M. Rho, Recent progress on dense nuclear matter in skyrmion approaches, Sci. China Phys. Mech. Astron. **60**, 032001 (2017).
[18] K. Nishiyama, S. Karasawa, and T. Tatsumi, Hybrid chiral condensate in the external magnetic field, Phys. Rev. D **92**, 036008 (2015).
[19] M. Buballa and S. Carignano, Inhomogeneous chiral symmetry breaking in dense neutron-star matter, Eur. Phys. J. A **52**, 57 (2016).
[20] H. Abuki, Chiral spiral induced by a strong magnetic field, EPJ Web Conf. **129**, 00036 (2016).
[21] H. Abuki, Chiral crystallization in an external magnetic background: Chiral spiral versus real kink crystal, Phys. Rev. D **98**, 054006 (2018).
[22] T. Maskawa and H. Nakajima, Spontaneous symmetry breaking in vector-gluon model, Prog. Theor. Phys. **52**, 1326 (1974).
[23] T. Maskawa and H. Nakajima, Spontaneous breaking of chiral symmetry in a vector-gluon model. II, Prog. Theor. Phys. **54**, 860 (1975).
[24] T. Kugo and M. G. Mitchard, The chiral Ward-Takahashi identity in the ladder approximation, Phys. Lett. B **282**, 162 (1992).
[25] T. Kugo and M. G. Mitchard, Calculating f_π in the consistent ladder approximation, Phys. Lett. B **286**, 355 (1992).
[26] M. Bando, M. Harada, and T. Kugo, External gauge invariance and anomaly in BS vertices and bound states, Prog. Theor. Phys. **91**, 927 (1994).
[27] B. R. He, Magnetic response of baryon properties in a Skyrme model, Phys. Rev. D **92**, 111503 (2015).
[28] M. Harada and K. Yamawaki, Hidden local symmetry at loop: A new perspective of composite gauge boson and chiral phase transition, Phys. Rep. **381**, 1 (2003).
[29] Y. L. Ma and M. Harada, Lecture notes on the Skyrme model, arXiv:1604.04850.
[30] M. Kugler and S. Shtrikman, A new skyrmion crystal, Phys. Lett. B **208**, 491 (1988).
[31] M. Kugler and S. Shtrikman, Skyrmion crystals and their symmetries, Phys. Rev. D **40**, 3421 (1989).
[32] A. S. Goldhaber and N. S. Manton, Maximal symmetry of the Skyrme crystal, Phys. Lett. B **198**, 231 (1987).
[33] M. Harada, H. K. Lee, Y. L. Ma, and M. Rho, Inhomogeneous quark condensate in compressed Skyrmion matter, Phys. Rev. D **91**, 096011 (2015).
[34] B. Y. Park, M. Rho, and V. Vento, Vector mesons and dense skyrmion matter, Nucl. Phys. A **736**, 129 (2004).
[35] V. P. Gusynin, V. A. Miransky, and I. A. Shovkovy, Dimensional reduction and catalysis of dynamical symmetry breaking by a magnetic field, Nucl. Phys. B **462**, 249 (1996).
[36] D. T. Son and M. A. Stephanov, Axial anomaly and magnetism of nuclear and quark matter, Phys. Rev. D **77**, 014021 (2008).
[37] M. Eto, K. Hashimoto, and T. Hatsuda, Ferromagnetic neutron stars: Axial anomaly, dense neutron matter, and pionic wall, Phys. Rev. D **88**, 081701 (2013).
[38] W. G. Paeng, T. T. S. Kuo, H. K. Lee, Y. L. Ma, and M. Rho, Scale-invariant hidden local symmetry, topology change, and dense baryonic matter. II, Phys. Rev. D **96**, 014031 (2017).
[39] Y. L. Li, Y. L. Ma, and M. Rho, The non-quenching of g_A in nuclei and emergent scale symmetry in dense baryonic matter, arXiv:1804.00310.
[40] Y. L. Ma, H. K. Lee, W. G. Paeng, and M. Rho, A pseudo-conformal equation of state in compact-star matter from topology change and hidden symmetries of QCD, arXiv:1804.00305.